Comprehensive analysis of electron correlations in three-electron atoms

Toru Morishita* and C. D. Lin
Department of Physics, Cardwell Hall, Kansas State University, Manhattan, Kansas 66506
(Received 11 August 1998)

We study the electron correlations in singly, doubly, and triply excited states of a three-electron atom. While electron correlation in general is weak for singly excited states, correlation plays major roles in determining the characteristics of doubly and triply excited states. Using the adiabatic approximation in hyperspherical coordinates, we show that the distinction between singly, doubly, and triply excited states is determined by the radial correlations, while finer distinctions within doubly or triply excited states lie in the angular correlations. Partial projections of the body-fixed frame wave functions are used to demonstrate the characteristic nodal surfaces which provide clues to the energy ordering of the states. We show that doubly excited states of a three-electron atom exhibit correlations that are similar to the doubly excited states of a two-electron atom. For the triply excited states, we show that the motion of the three electrons resemble approximately that of a symmetric top. [S1050-2947(99)03902-5]

PACS number(s): 31.10.+z, 31.15.Ja, 31.25.Jf

I. INTRODUCTION

The structure of atoms has been studied since the early days of quantum mechanics. Traditionally, the basic conceptual framework for describing a many-electron atom is the independent electron model. In this model each electron can occupy one of the many available ''orbitals'' which are determined by a variational procedure such as the Hartree-Fock approximation. The deviation of the properties of a many-body system from the independent electron approximation often is small such that the deviation can be treated by perturbation theories or the configuration-interaction (CI) approach. In fact, it is a common practice to define correlation energy as the difference between the ''exact'' energy from the prediction of the Hartree-Fock approximation. This common practice is unfortunate since it fails completely to address the major issue of electron correlation which is the description of how the motion of electrons in the system is interrelated. Such information is contained in the many-electron wave function, not in the ''correlation energy.''

It is well known that the independent electron approximation fails to describe the doubly excited states of two-electron atoms such as He and H^-. In the past two decades, major progress has been made on understanding the nature of electron correlations in doubly excited states. Equivalent descriptions for these doubly excited states have been provided and a set of new approximate quantum numbers has been proposed [1–5]. In all of these descriptions the motion of the two electrons is treated together and the correlation between the two electrons is understood as analogous to the vibration and rotation of a flexible linear triatomic molecule. It is fair to say that correlations in doubly excited states of a two-electron atom are now well understood.

The success of describing correlations in doubly excited states in a two-electron atom poses two new questions. First, do doubly excited states of a many-electron atom resemble those of a two-electron atom? In what way is the description to be modified for doubly excited states of a many-electron atom? Second, can one make the next step to understand the correlation of triply excited states? Both questions can be addressed by studying the doubly and triply excited states of a three-electron atom, such as the Li atom.

From the theoretical viewpoint, doubly excited states and triply excited states are very difficult to treat. First, their energies lie way above the ground state and the lower singly excited states where various variational methods have been successfully applied. Second, the spectral density of these multiply excited states is very large. While it is of interest to do specific calculations for individual states, one of the most urgent needs is to obtain a global understanding and organization of these states. This amounts to identifying common features as well as features that distinguish them, with the ultimate goal of being able to find a new set of quantum numbers for their classification. Since electron correlation is known to play a major role in determining the nature of multiply excited states, the delineation of their wave functions is the first step toward this goal. However, this cannot be easily done for many-particle systems. For an N-electron atom, the spatial part of the wave function is described by a $3N$-dimensional function. Visualization of such a function with two-dimensional projection in a manner which would reveal information on how the electrons are correlated is thus nearly impossible. We comment that the standard procedure of calculating the two-body or even three-body correlation functions is not very useful unless one happens to have the ''right'' variables for displaying the essential features. Thus the search for understanding electron correlations amounts to finding the ultimate method of displaying the multidimensional wave functions. Different variables and different procedures will be used to display the correlation of doubly and triply excited states.

In this paper we address the correlation properties of doubly excited states and of triply excited states of a Li atom within the adiabatic approximation using hyperspherical coordinates. The hyperspherical approach has been used very

*Present address: Department of Applied Physics and Chemistry, the University of Electro-communications, 1-5-1, Chofu-ga-oka, Chofu-shi, Tokyo 182-8585, Japan.

successfully for understanding electron correlations in doubly excited states of a two-electron atom. Very accurate computational procedures have also been developed using a hyperspherical approach [6–11]. In Sec. II we first briefly summarize the computational methods from which the whole spectrum of the singly, doubly, and triply excited states can be calculated. In Sec. III we show the calculated adiabatic potentials to see global features of three-electron atoms. In Sec. IV we show that singly, doubly, and triply excited states are distinguished by this nodal structure and the distributions of the wave function in the two hyperangles. The correlation properties of doubly excited states will be examined in Sec. V where it will be shown that their properties are similar to the doubly excited states of a two-electron atom. The correlation properties of triply excited states will be examined in Sec. VI.

II. HYPERSPHERICAL METHOD FOR THREE-ELECTRON ATOMS

The details of the computational method have been presented previously [12]. In this section we only outline the essential steps.

The Schrödinger equation for a three-electron atom in the independent particle coordinates is given by (in atomic units)

$$\left[\sum_{i=1}^{3}\left(-\frac{1}{2}\nabla_i^2-\frac{Z}{r_i}\right)+\sum_{i<j}\frac{1}{|\mathbf{r}_i-\mathbf{r}_j|}-E\right]\Psi(\mathbf{r}_1,\mathbf{r}_2,\mathbf{r}_3)=0, \tag{1}$$

where Z is the nuclear charge and E is the total energy measured from the triple ionization threshold. The hyperspherical method replaces the radial distances r_1, r_2, and r_3 of the three electrons from the nucleus by the hyperradius R and two angles α_1, α_2 defined by

$$\begin{aligned} r_1 &= R\sin\alpha_2\cos\alpha_1, \\ r_2 &= R\sin\alpha_2\sin\alpha_1, \\ r_3 &= R\cos\alpha_2, \end{aligned} \tag{2}$$

where R stands for the size of the system, and α_1 and α_2 measure the relative distances of the electrons from the nucleus—they are the variables for measuring radial correlations. In the calculation of the wave functions, we use the spherical angles $\hat{\mathbf{r}}_i=(\theta_i,\phi_i)$ $(i=1,2,3)$ of each electron in the space-fixed frame. (We will use other sets of angles in the body-fixed frame to analyze the wave functions, see Secs. V and VI.) Thus the nine-dimensional spatial coordinates of the three electrons in the space-fixed frame are represented by the hyperradius R and eight hyperangles $\{\alpha_1,\alpha_2,\hat{\mathbf{r}}_1,\hat{\mathbf{r}}_2,\hat{\mathbf{r}}_3\}$, where we shall use Ω at times to denote all the eight hyperangles collectively. In hyperspherical coordinates the Schrödinger equation for the rescaled wave function $\psi=Rr_1r_2r_3\Psi$ is

$$\left[-\frac{1}{2}\frac{\partial^2}{\partial R^2}+H_{\rm ad}(\Omega;R)-E\right]\psi(R,\Omega)=0, \tag{3}$$

where $H_{\rm ad}(\Omega;R)$ is the adiabatic Hamiltonian defined at fixed hyperradius R.

Within the adiabatic approximation [13] the total wave function for the nth state in channel μ can be written as

$$\psi(R,\Omega)=F_\mu^n(R)\left(\sum_{S_{12}}\Phi_\mu^{S,S_{12}}(\Omega;R)\chi_{S_{12}}^S\right), \tag{4}$$

where $F_\mu^n(R)$ is the hyperradial function, which measures the size of the system; Φ_μ is the hyperspherical adiabatic channel function, which contains all the information about electron correlations for states within channel μ; and $\chi_{S_{12}}^S=[\{\chi(1)\chi(2)\}^{S_{12}}\chi(3)]^S$ is the total spin function with intermediate spin S_{12}. The channel function Φ_μ and its associated adiabatic potential $U_\mu(R)$ are obtained by solving the adiabatic eigenvalue problem at each R,

$$[H_{\rm ad}(\Omega;R)-U_\mu(R)]\Phi_\mu(\Omega;R)=0. \tag{5}$$

Equation (5) is a partial differential equation of the eight angles Ω. To solve this equation, we use the eigenfunctions of the adiabatic Hamiltonian which contains only the nucleus-electron attractive potential as the basis set. These eigenfunctions can be written in the separable form,

$$\tilde{\Phi}_\mu^\gamma(\Omega;R)=g_\mu^\gamma(\alpha_1,\alpha_2;R)\mathcal{Y}_\gamma^{LM}(\hat{\mathbf{r}}_1,\hat{\mathbf{r}}_2,\hat{\mathbf{r}}_3), \tag{6}$$

where $\gamma=\{l_1l_2l_3l_{12}\}$, and $\mathcal{Y}_\gamma^{LM}(\hat{\mathbf{r}}_1,\hat{\mathbf{r}}_2,\hat{\mathbf{r}}_3)=[\{Y_{l_1}(\hat{\mathbf{r}}_1)\,Y_{l_2}(\hat{\mathbf{r}}_2)\}^{l_{12}}Y_{l_3}(\hat{\mathbf{r}}_3)]^{LM}$ is the coupled angular momentum of the three electrons. The function $g_\mu^\gamma(\alpha_1,\alpha_2;R)$ satisfies the two-dimensional eigenvalue problem with respect to α_1 and α_2 which is then diagonalized using direct products of discrete variable representation (DVR) basis sets [14]. In Eq. (4), the spatial part of the channel function $\Phi_\mu^{S,S_{12}}$ is coupled to the spin functions. In constructing the total wave function ψ the Pauli exclusion principle has to be accounted for. To obtain the correct symmetry under exchange of any pair of electrons, we apply the antisymmetrization operator to the basis functions in Eq. (6), and then diagonalize the adiabatic Hamiltonian with these antisymmetrized basis functions. In our calculations, we include angular configurations of $l_i\leqslant 3$ for each electron. The resulting adiabatic potentials and channel functions are accurate enough for the analysis of electron correlations in the present work.

III. HYPERSPHERICAL ADIABATIC POTENTIAL CURVES

To see the global features of the eigenstates of a three-electron atom, we first examine the adiabatic potentials. In Fig. 1 we show the potential curves $U_\mu(R)$ as functions of R calculated for Li($^2P^o$) as an example. The top figure gives the overall view of the potential curves. At large R, each curve approaches the two-electron (Li^+) limits. The lowest curve goes to the ground state of Li^+ in the asymptotic limit. This curve supports the singly excited states of Li. All the singly excited states which are normally designated as $1s^2np\,^2P^o$ are obtained by solving the hyperradial equation from this curve.

The next group of curves approaches the singly excited states of Li^+ asymptotically. In the lower-left frame we show the first few of them, where the first six curves converge to the $1s2s\,^3S^e$, $1s2s\,^1S^e$, $1s2p\,^3P^o$, and $1s2p\,^1P^o$ limits of Li^+ at large R. These curves support doubly excited states

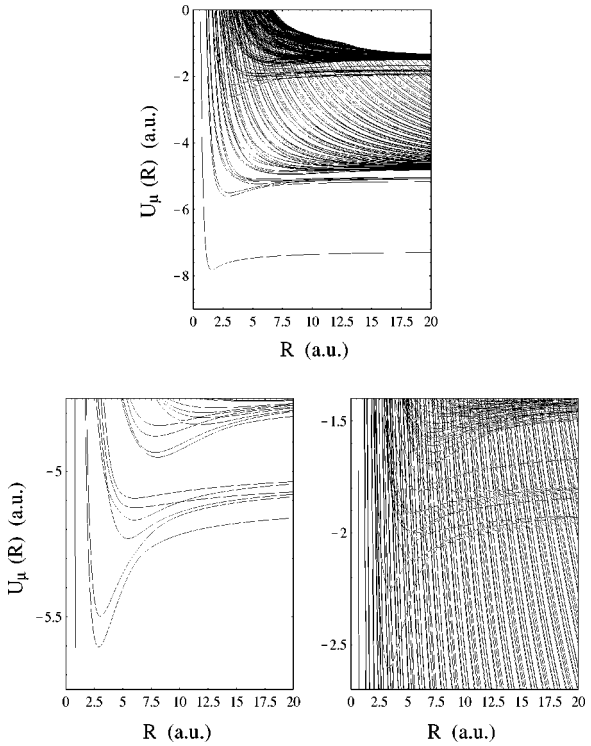

FIG. 1. Adiabatic hyperspherical potentials for the $^2P^o$ symmetry of Li. Top frame: the complete set; lower-left frame: expanded view of the adiabatic potentials that support $1s2nl'$ doubly excited states and some curves that support $1s3lnl'$ doubly excited states; lower-right frame: expanded view of the adiabatic potentials that support $2l2l'2l''$ triply excited states and some curves that support $2l3l'nl''$ triply excited states. These curves have sharp avoided crossings with steep curves that support doubly excited states.

which are designated as $1s2lnl'$, implying that these states lie below the $1s2l$ singly excited states of Li^+. The higher adiabatic potentials of this group support doubly excited states of the type $1s3lnl'$, $1s4lnl'$, etc.

In the lower-right corner of Fig. 1 we show the third group of adiabatic potentials. These potentials exhibit numerous sharp avoided crossings with the curves that support doubly excited states. The doubly excited curves drop rapidly with increasing values of R, while the curves in the third group show clear attractive wells in the small R region. These curves approach the doubly excited states of Li^+ asymptotically, and they support triply excited states of Li. In the third group, the lowest nine curves approach the $2l2l'$ doubly excited states of Li^+ such that they support $2l2l'nl''$ triply excited states of Li.

From the discussion above it is clear that the hyperspherical adiabatic potentials can be used to separate singly, doubly, and triply excited states. In fact, for the low-lying members of doubly excited states and triply excited states, the adiabatic potentials allow us to separate the eigenstates into $(1,1,n)$, $(1,2,n)$, $(1,3,n)$, . . . and $(2,2,n)$,$(2,3,n)$, . . . , $(3,3,n)$ manifolds. Within each manifold, there are many channels or Rydberg series. The adiabatic potentials clearly illustrate that there are hierarchical ordering in the energy levels — that the states are separated into manifolds and then into different Rydberg series. Our major goal in this paper is to identify features that characterize the different manifolds as well as features that distinguish the different

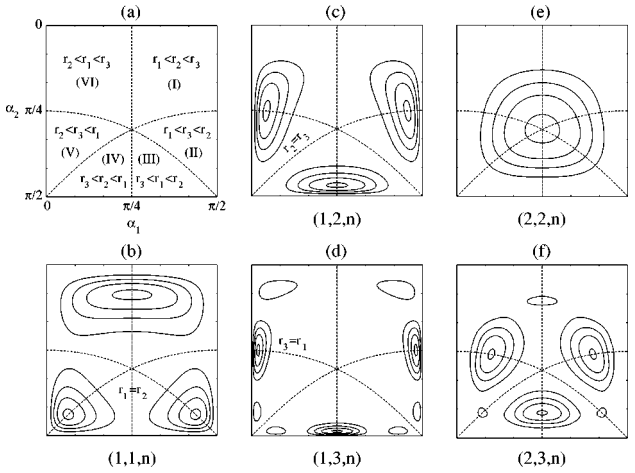

FIG. 2. Radial density functions $\rho^{\mu}_{\rm rad}(\alpha_1,\alpha_2;R)$ on the (α_1,α_2) plane at fixed R. (a) the six equivalent domains where the relative magnitudes of the radial distances of the electrons are indicated. The dashed lines indicate where the radial distances of two of the electrons are equal, see (b)–(d). The point where the three dashed lines cross is for $r_1=r_2=r_3$. The radial densities $\rho_{\rm rad}(\alpha_1,\alpha_2;R)$ are shown (b) for the $1s^2nl$ singly excited states at $R=2$ a.u.; (c) for the $1s2lnl'$ doubly excited states at $R=3.5$ a.u.; (d) for the $1s3lnl'$ doubly excited states at $R=8$ a.u.; (e) for the $2l2l'nl''$ triply excited states at $R=3.5$ a.u.; and (f) for the $2l3l'nl''$ triply excited states at $R=7$ a.u.

channels within the same manifold. At this point we need to point out that overlap of states from different manifolds can happen for the higher manifolds of doubly excited states and of triply excited states. Such overlapping resonances from different manifolds are known in doubly excited states of He both experimentally [15] and theoretically [16].

IV. RADIAL CORRELATIONS

We first define the radial density function which is obtained by integrating the modulus square of the channel functions over all the six spherical angles $\hat{\mathbf{r}}_i$ $(i=1,2,3)$ and summing over the intermediate spin S_{12}, namely,

$$\rho^{\mu}_{\rm rad}(\alpha_1,\alpha_2;R)=\sum_{S_{12}}\int|\Phi^{S,S_{12}}_{\mu}(\Omega;R)|^2 d\hat{\mathbf{r}}_1 d\hat{\mathbf{r}}_2 d\hat{\mathbf{r}}_3. \quad (7)$$

This function gives the radial distributions of the three electrons at each hyperradius R. We first show that the manifolds are distinguished by the distributions of the radial density function $\rho^{\mu}_{\rm rad}(\alpha_1,\alpha_2)$. In Fig. 2(a) we divide the (α_1,α_2) plane into six domains, or sextants, which are labeled by (I)–(VI) and separated by the dotted lines where the radial distances of two of the electrons are identical [indicated explicitly in Figs. 2(b)–2(d)]. The point where the three dotted lines intersect is for $r_1=r_2=r_3$. Since the densities of the three-electron wave functions are symmetric under the exchange of any two electrons, the radial density function distribution within each domain is equivalent to that for the other five.

In Fig. 2(b) we first show the density plot for the $1s^2nl$ singly excited states at $R=2$ a.u., where the potential (the lowest curve of Fig. 1) is near the minimum. We will focus

on sextant (I) or (VI), where r_3 is larger than both r_1 and r_2. The peak of this distribution is at $(\alpha_1,\alpha_2)\approx(\pi/4,\pi/12)$. Since $R=2$ a.u., this gives $r_1=r_2\approx 0.4$ a.u. and $r_3\approx 1.9$ a.u., which gives roughly the radial distances of the three electrons in the $1s^2 2p$ state.

In Fig. 2(c), it is more convenient to examine sextant (III) or (IV), where r_3 is the smallest. The peak occurs at $(\alpha_1,\alpha_2)\approx(\pi/4,17\pi/36)$. Since $R=3.5$ a.u., this gives $r_3\approx 0.3$ a.u. and $r_1=r_2\approx 2.5$ a.u., thus representing a $1s2l2l'$ doubly excited state. In Fig. 2(d), the peaks in sextant (III) or (IV) indicate that the maximum of the density is at $r_3\approx 0.3$ a.u., $r_1=r_2\approx 5.7$ a.u. Therefore this represents the radial distribution of a $1s3l3l'$ doubly excited state. Comparing Figs. 2(c) and 2(d) in sextant (IV), we note that there is an additional approximate nodal line in $\alpha_1\approx\pi/8$ in Fig. 2(d). This is easily understood since the $1s3l3l'$ doubly excited states have one additional nodal line in the hyperangle α_1.

The same procedure can be used to understand that Fig. 2(e) represents $2l2l'2l''$ triply excited states where the density peaks at $r_1=r_2=r_3\approx 1.9$ a.u. and that Fig. 2(f) represents a $2l3l'3l''$ triply excited state, see sextant (I) or (VI) where the peak occurs at $r_1=r_2\approx 4.8$ a.u. and $r_3\approx 1.8$ a.u.

The results in Fig. 2 clearly establish that the different manifolds of singly, doubly, and triply excited states can be distinguished by the radial distributions of the wave functions. We have shown the results only for the $^2P^o$ states, but the conclusion is expected to be true for other symmetries. Thus to characterize the radial correlations of the three electrons, meaning to describe the relative distances of the three electrons from the nucleus, it is possible to use the manifold designations. We note that the hierarchical structure in radial correlation has been discussed in the sense of the hierarchy of the adiabatic separation between the hyperradial variables [17].

V. CORRELATIONS IN DOUBLY EXCITED STATES OF LI

We next address what distinguishes the different channels in a given manifold. Although there are some differences in the radial density function $\rho^{\mu}_{\rm rad}(\alpha_1,\alpha_2;R)$ among the channels within the same manifold on the (α_1,α_2) plane, the major differences are in the relative angles among the electrons. In this section, we focus on the $1s2lnl'$ doubly excited states of Li.

From the lower corner of Fig. 1, the lowest six adiabatic potential curves support the $1s2lnl'$ doubly excited states of Li ($^2P^o$). The six Rydberg series can be designated as $1s2s(^3S^e)np$, $1s2s(^1S^e)np$, $1s2p(^3P^o)ns$, $1s2p(^3P^o)nd$, $1s2p(^1P^o)ns$, and $1s2p(^1P^o)nd$ series in the independent electron approximation. The designation above is inadequate since the mixing of the series is expected to be very strong, as in the case of doubly excited states of He. In fact, we can compare the six adiabatic potentials with the three $^1P^o$ and three $^3P^o$ adiabatic potentials of He ($N=2$), where each curve can be labeled by the $(K,T)^A$ quantum numbers [1–4]. The adiabatic potentials in the two systems are very similar in the small R region where the two outer electrons are strongly correlated, and the approximate quantum numbers used to describe the doubly excited states of He can be used to label the doubly excited states of Li. However, for the higher states of each Rydberg series, the outermost electron decouples from the two inner ones which form the $1s2s\,^3S^e$, $1s2s\,^1S^e$, $1s2p\,^3P^o$, or $1s2p\,^1P^o$ series limits of Li^+. For the helium atom, the asymptotic limit is either the $2s$ or the $2p$ states of He^+ which are degenerate. Thus the adiabatic potentials in the large R region for the two systems are different.

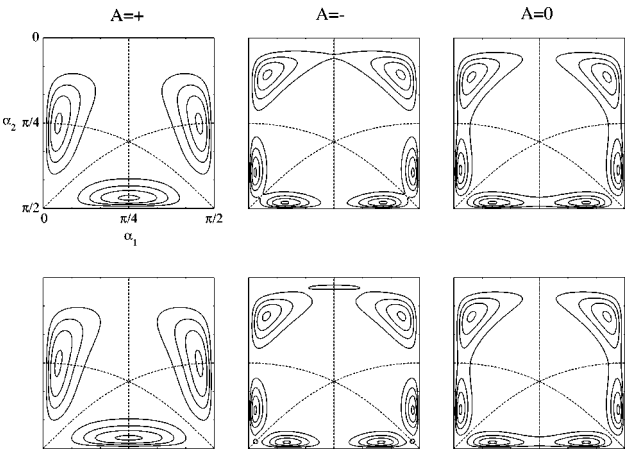

FIG. 3. The radial density functions $\rho_{\rm rad}(\alpha_1,\alpha_2)$ for the six $1s2lnl'\,^2P^o$ channels of Li. The leftmost column shows the two $A=+$ channels at $R=3$ a.u. The middle column shows the $A=-$ channels at $R=6$ a.u. The rightmost column shows the two $A=0$ channels at $R=6$ a.u.

To show the correlation of the two outer electrons in a three-electron atom, the integrated density plots $\rho_{\rm rad}(\alpha_1,\alpha_2;R)$ are not the most illustrative. However, we will show the $\rho_{\rm rad}(\alpha_1,\alpha_2;R)$ plots for all six channels to demonstrate their similarities and their ''minor'' differences. In Fig. 3 the first two figures in the left column give the density plots of the two lowest potentials of Fig. 3(a). Both belong to the $A=$''$+$'' channels. Consider the plots in sextant (III) or (IV). In these domains, r_3 is the smallest, and the maxima of the density plots occur at $r_1=r_2$, illustrating that they represent intrashell doubly excited states. Comparing to the two figures in the middle column, the density plots in the same region show little magnitude along the $r_1=r_2$ line. These two frames represent the ''$-$''-type doubly excited states where the wave function vanishes at $r_1=r_2$ or at $\alpha_1=\pi/4$. In Fig. 3 the two frames in the far right column show the radial density plots for the two $A=$''0'' channels. These states have small amplitudes in the $\alpha_1=\pi/4$ region, but $\alpha_1=\pi/4$ is not a nodal line.

A clearer illustration of doubly excited states is to show the correlation between the two doubly excited electrons. A similar illustration has been made by Le Dourneuf and Watanabe [18] for He^- in the grandparent model where they treated the effect of the innermost electron by adding a surface operator to the two-electron Hamiltonian. In our treatment, this is done by fixing $r_3 \ll r_1, r_2$ [or fixing $\alpha_2\sim 0$, see Eq. (2)] and integrating over $\hat{r}_3$. We define the two-electron density function for the two excited electrons on the (α_1,θ_{12}) plane by

$$\rho_{2e}(\alpha_1,\theta_{12};\alpha_2,R)=\sum_{S_{12}}\int |\Phi_{\mu}^{S,S_{12}}(\Omega;R)|^2 d\hat{\mathbf{r}}_3 d\omega, \quad (8)$$

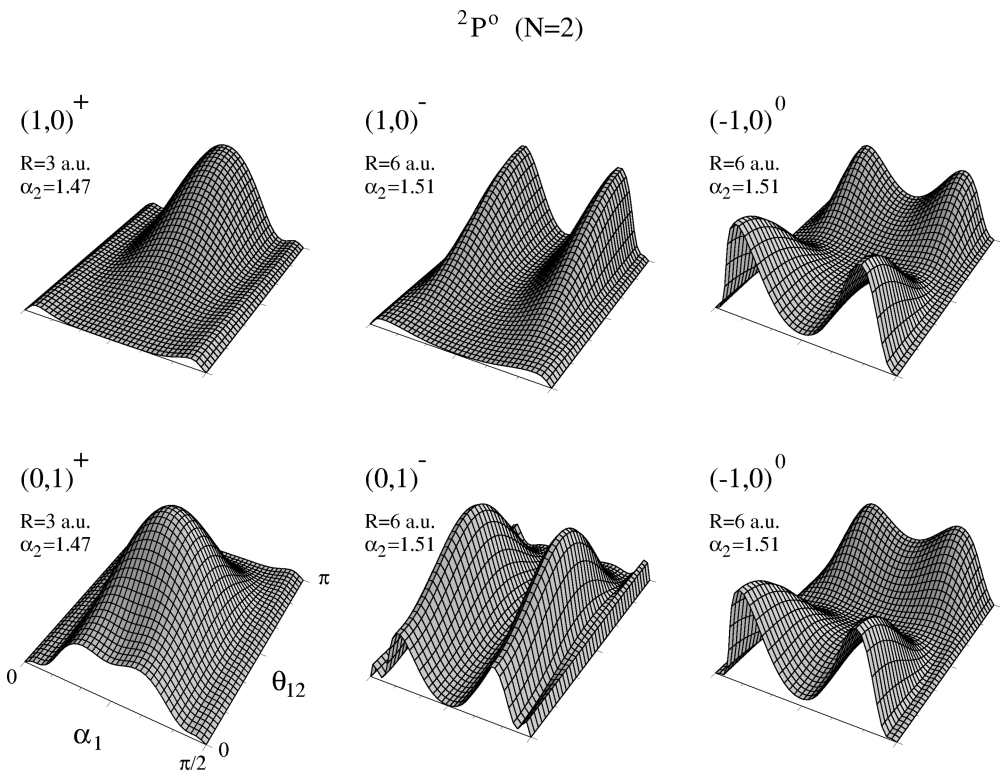

FIG. 4. The rotation-averaged density of the two excited electrons $\rho_{2e}(\alpha_1,\theta_{12};\alpha_2,R)$ on the (α_1,θ_{12}) plane for the six $1s2lnl'\ ^2P^o$ channels of Li. Each density is evaluated at the values of R and α_2 shown and labeled by the $(K,T)^A$ quantum numbers used previously for the doubly excited states of two-electron atoms.

where θ_{12} is the angle between $\mathbf{r}_1$ and $\mathbf{r}_2$, and $d\omega$ is the volume element for the three Euler angles used to describe the overall rotation of the whole atom. The resulting two-electron density plots for the six $1s2lnl'$ doubly excited series of Li are shown in Fig. 4. They are essentially the same as the correlation patterns of doubly excited states of a two-electron atom like He or Li^+. The top frame of the left column resembles the $(1,0)^+\ ^3P^o$ channel of the $N=2$ doubly excited states of He. It is characterized by having the maximum density at $\alpha_1=\pi/4$ and $\theta_{12}=\pi$. The lower frame of the left column is identical to the $(0,1)^+\ ^1P^o$ channel of the $N=2$ doubly excited states of He. The density peaks at $\alpha_1=\pi/4$ but the maximum in θ_{12} is at a smaller angle away from π. Other figures in Fig. 4 show the correlation pattern characteristic of the doubly excited states of two-electron atoms and are labeled by the $(K,T)^A$ quantum numbers indicated. Le Dourneuf and Watanabe showed similar features for doubly excited states of He^- and H^- [18]. The correlation properties of doubly excited states of Li are shown to be similar to those in the doubly excited states in He and can be labeled by the same set of K, T, and A quantum numbers.

VI. CORRELATION IN TRIPLY EXCITED STATES OF LI

To study the correlation properties in triply excited states, clearly the three electrons are to be treated on an equal footing. We first discuss the theoretical framework for displaying and analyzing the correlations for intrashell triply excited states. We then show the results for the $2l2l'2l''$ intrashell states of Li.

A. Body-frame analysis of the channel wave functions

Since correlation is a property of the relative motions among the electrons, the overall rotation of the system does not play a role. Thus we analyze the wave functions in the body-fixed frame of the atom.

The channel function $\Phi^{S,S_{12}}_{\mu LM}(\Omega;R)$ in the space-fixed frame can be expressed in terms of channel functions $\varphi^{S,S_{12}}_{\mu LQ}(\Omega_I;R)$ in the body-fixed frame by a general rotation

$$\Phi^{S,S_{12}}_{\mu LM}(\Omega;R)=\sum_{Q=-L}^{L}\varphi^{S,S_{12}}_{\mu LQ}(\Omega_I;R)D^{(L)}_{QM}(\omega), \qquad (9)$$

where $D^{(L)}_{QM}(\omega)$ is the rotation matrix for the frame transformation, and Q and M are the azimuthal components of L in the body-fixed frame and in the space-fixed frame, respectively. Here we use ω for the three Euler angles which represent the orientation of the atom, and the notation Ω_I for the five internal angles which represent the ''shape'' of the system. There are many different ways to choose the internal coordinates. Mathematical details on the internal coordinates for the general four-body system have been studied in Ref. [19]. In the present analysis of the triply excited states of a three-electron atom, we use α_1, α_2, and three relative angles among the electrons. Let us define the three relative angles θ, η, and ϕ. For $r_1=r_2=r_3$, the three electrons lie on the surface of a sphere. We define a σ plane formed by the three electrons. This plane makes an angle θ with respect to the nucleus, see Fig. 5(a). On the σ plane, the three electrons lie on a circle. The angle between electrons 1 and 2 is defined to be 2η, choosing the arc containing electron 3. The

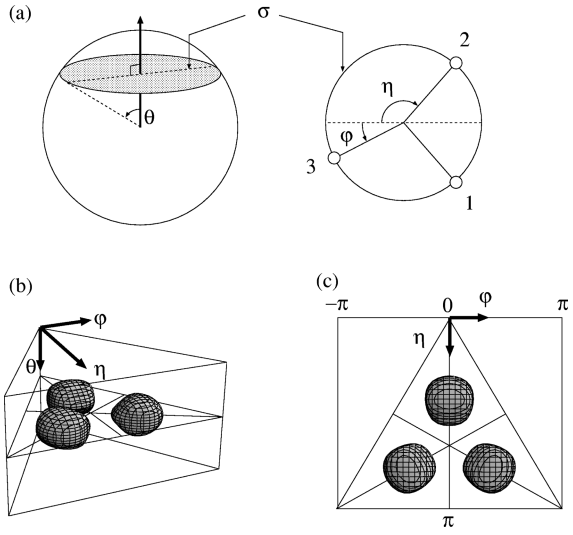

FIG. 5. (a) Definition of the three angles used to describe the three electrons on a sphere. The three electrons form a σ plane. On the plane (the right figure) the three electrons are confined to a circle. (b) Side view and (c) top view of the equidensity surface plots of the three-electron density functions $\rho^{\mu}_{3e}(\Omega_I;R)$ for a typical intrashell triply excited state of Li at $r_1=r_2=r_3$. The surface represents 60% of the maximum density. Each ''slice'' represents the whole range of the three angles ($0\leqslant\theta\leqslant\pi$, $0\leqslant\eta\leqslant\pi$, $-\eta\leqslant\phi\leqslant\eta$).

angle between electron 3 and the line bisecting electrons 1 and 2 is defined to be ϕ, see Fig. 5(a). The ranges of the angles are ($0\leqslant\theta\leqslant\pi$, $0\leqslant\eta\leqslant\pi$, $-\eta\leqslant\phi\leqslant\eta$). These three angles specify a definite shape of the triangle and the position of the triangle with respect to the nucleus.

To visualize the collective motion of the three electrons, we introduce the three-electron density function $\rho^{\mu}_{3e}(\Omega_I;R)$ which is defined as the rotation-averaged density distribution for each channel function,

$$\rho^{\mu}_{3e}(\Omega_I;R)=\sum_{S_{12}}\int|\Phi^{S,S_{12}}_{\mu}(\Omega;R)|^2 d\omega. \tag{10}$$

This density represents the probability for the three electrons to take specific shapes. From Fig. 2(e) it has been shown that each intrashell state wave function peaks at $r_1=r_2=r_3$ at the value of R where the potential is near the minimum. Thus the correlation of the three electrons at $r_1=r_2=r_3$ is expected to represent the dominant correlation properties of intrashell triply excited states. In Fig. 5(c) we show the density for an intrashell state of Li at $r_1=r_2=r_3$ as an example. Since each density still depends on three internal angles, θ, η, and ϕ, it is not easily displayed for visualization. To display the global feature of a function in three dimensions we use ''equidensity surfaces'' which are a surface of constant electronic density. The plots in Fig. 5(b) and Fig. 5(c) represent the contour surfaces where the density is 60% of the maximum. A contour surface of higher density would fit inside the surface. Such contour surfaces would provide information on the most probable shape of the three electrons in each intrashell triply excited state.

Next we consider the rotational decomposition of the wave functions of triply excited states. In Eq. (9), the channel function of each Q component $\varphi^{S,S_{12}}_{\mu LQ}$ depends on the choice of the body-frame axes. Following Ref. [20] we define our body frame by

$$\begin{aligned}\mathbf{S}_z&=\mathbf{r}_1\times\mathbf{r}_2+\mathbf{r}_2\times\mathbf{r}_3+\mathbf{r}_3\times\mathbf{r}_1,\\ \mathbf{S}_y&=\frac{\sqrt{3}}{2}(\mathbf{r}_1-\mathbf{r}_2),\\ \mathbf{S}_x&=\mathbf{S}_y\times\mathbf{S}_z.\end{aligned} \tag{11}$$

This defines the z axis on the body frame to be perpendicular to the plane spanned by the three electrons. Namely, we consider a three-electron atom as an oblate molecule. In the body-fixed frame, the channel functions satisfy the relation [20]

$$\varphi_{\mu L-Q}(\Omega_I;R)=\pi(-1)^{L+Q}\varphi^{*}_{\mu LQ}(\Omega_I;R), \tag{12}$$

where $\pi=\pm1$ is the parity of the system. We take $T=|Q|$ $(0\leqslant T\leqslant L)$ for analysis in what follows. Quantum symmetries often impose boundary conditions on each rotational component wave function. More specifically, each quantum state with well-defined rotational symmetry, well-defined parity, as well as Pauli exchange symmetry between each pair of electrons has nodal surfaces on the wave functions in the body-fixed frame. For the body-fixed frame defined by Eq. (11), Watanabe and Lin [20], and Bao *et al.* [21] have shown the following conditions that the internal wave functions vanish because of their quantum symmetries.

(1) For

$$\pi(-1)^T=-1, \tag{13}$$

the wave function vanishes at the coplanar geometry of the three electrons with nucleus ($\theta=\pi/2$).

(2) For

$$\begin{aligned}&T=1,2,\quad \mathrm{mod}\ 3\quad (S=3/2),\\ &T=0,\quad \mathrm{mod}\ 3\quad (S=1/2),\end{aligned} \tag{14}$$

the wave function has a nodal surface when the three electrons form an equilateral triangle ($\eta=2\pi/3$, $\phi=0$) with $r_1=r_2=r_3$.

(3) For

$$\pi(-1)^L=1\quad (T=0,S=3/2), \tag{15}$$

the wave function has a nodal surface when the three electrons form an isosceles triangle ($\phi=0$) with $r_1=r_2=r_3$.

These nodal surfaces will be seen in the density function if there is only one rotational component represented by

$$\rho_{3e}^{\mu,T}(\Omega_I;R)=\begin{cases}\displaystyle\sum_{S_{12}}|\varphi_{\mu LT}^{S,S_{12}}(\Omega_I;R)|^2 \quad (T=0)\\ \rho_{3e}^{\mu,T}(\Omega_I;R)=\displaystyle\sum_{S_{12}}(|\varphi_{\mu L-T}^{S,S_{12}}(\Omega_I;R)|^2+|\varphi_{\mu LT}^{S,S_{12}}(\Omega_I;R)|^2) \quad (T\neq 0).\end{cases} \tag{16}$$

We will show the partial densities for a number of triply excited states in the next subsection, but we note that there are no examples for condition (3) above for the $2l2l'2l''$ states.

For a rigid body T is a good quantum number. One of the possible measures of how ''rigid'' the three electrons are moving together can be obtained by determining whether T is nearly a good quantum number for the given state. We define the partial normalization constant of each rotational component by integrating over all the five internal coordinates,

$$N_T(R)=\frac{1}{8\pi^2}\int \rho_{3e}^{\mu,T}(\Omega_I;R)d\Omega_I, \tag{17}$$

where

$$\sum_{T=0}^{L} N_T(R)=1 \tag{18}$$

at each R. For the calculation of the above integral, we take the five coordinates to be $(\alpha_1,\ \alpha_2,\ \cos\theta_{12}=\hat{\mathbf{r}}_1\cdot\hat{\mathbf{r}}_2,\ \cos\theta_{31}=\hat{\mathbf{r}}_3\cdot\hat{\mathbf{r}}_1,\ \phi_{23}=\phi_3-\phi_2)$, which are different from the variables for the density plots. In this coordinate system, $d\Omega_I=d\cos\alpha_1 d\alpha_2 d\cos\theta_{12} d\cos\theta_{31} d\phi_{23}$ and the five-dimensional (5D) integration is performed numerically. There is no *a priori* reason to expect that the three electrons move like a rigid body. However, if there is a T component which is nearly pure, meaning that $N_T(R)$ is nearly equal to one, then there is a possibility that the motion of the three electrons will be close to that of a rigid body. Similar investigations have been done for doubly excited states for two-electron systems [5,18,22].

B. Demonstration of rotor structure of intrashell triply excited states

The total three-electron density for each of the eight $2l2l'2l''$ intrashell triply excited states has been reported previously [23]. In Fig. 6 we show the rotational decomposition into the T components for each state. Each plot in Fig. 6 represents the contour surface where the density is 60% of the maximum at fixed $r_1=r_2=r_3=2.02$ a.u. ($R=3.5$ a.u.). The fraction of each T-component with respect to the total density for each state is also indicated in the figure. [This is done by integrating the partial density $\rho_{3e}^{\mu,T}$ over the three relative angles $(\theta_{12},\theta_{31},\phi_{23})$ at fixed $r_1=r_2=r_3$.]

Let us consider the first four states, $^4P^e$, $^2P^o$, $^2D^o$, and $^2D^e$. The total density $\rho_{3e}^{\mu}(\Omega_I;R)$ for each state, as shown in the rightmost column of Fig. 6, clearly indicates that they are essentially identical. In fact, the maximum of the density for each state occurs at $\theta=\pi/2$, $\eta=2\pi/3$, and $\phi=0$. That is, the most favorable geometry of the three electrons is a coplanar equilateral triangle with the nucleus at the center. Also, clearly each state has a single dominant T component, and this T component has the coplanar equilateral triangle geometry for the three electrons. The existence of a single dominant T component and that this component has nearly identical shape underlies the basis of the classification of these states as similar to the rotor structure of an oblate symmetric top. From Fig. 6, it is clear that the purity is very good for the low-lying $^4P^e$ and $^2P^o$ states. For the highest $^2D^o$ state the fraction of the nondominant T components is not small, and the total density for the $^2D^o$ state is somewhat ''irregular.'' From the molecular physics viewpoint, this large mixture is interpreted as due to the rotation-vibrational

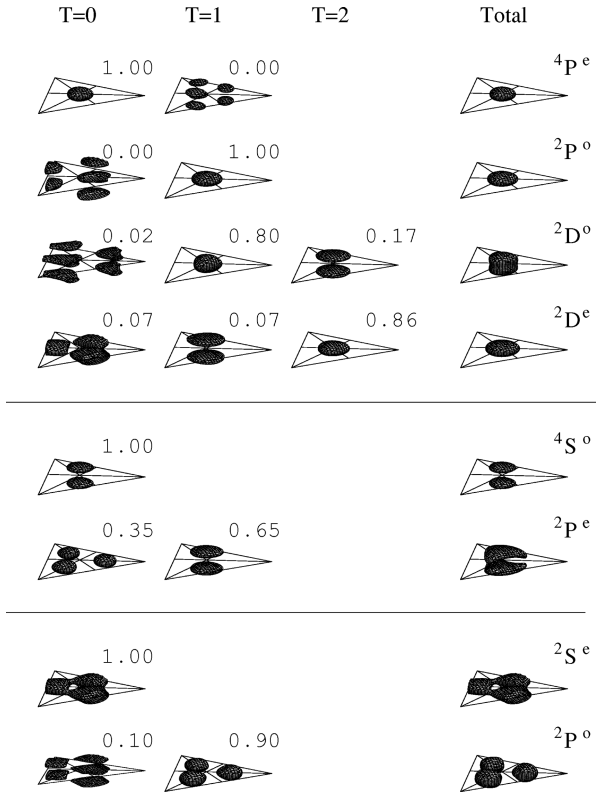

FIG. 6. The equidensity surface plots of the three-electron density functions $\rho_{3e}^{\mu}(\Omega_I;R)$ for the eight intrashell $2l2l'2l''$ triply excited states of Li at $r_1=r_2=r_3=3.5$ a.u. The total density is shown in the rightmost column while the density for each rotational T component is shown to the left. The fraction of each T component is indicated to denote the purity of that component for a given state. (If the fraction is less than 10^{-2}, it is listed as 0.00.) The surface represents 60% of the maximum density.

coupling which becomes important for states with higher angular momentum.

The next group consists of the $^4S^o$ state and the $^2P^e$ state. The $^4S^o$ state has the $T=0$ component only and it has a nodal plane at $\theta=\pi/2$, i.e., this state satisfies Eq. (13). For the $^2P^e$ state, the $T=1$ component has a node at $\theta=\pi/2$ but the $T=0$ has a node at the coplanar equilateral triangle geometry [see Eq. (14)]. Since each component has a nodal surface, the two T components have nearly identical composition and thus the purity of this state is not good, as shown by the fraction of each rotational component and the ''irregular shape'' in the total density.

The last group consists of the $^2S^e$ state and the second $^2P^o$ state. The $^2S^e$ state has one nodal surface at the equilateral triangle geometry. This is also true for the $T=1$ component of the second $^2P^o$ state. We note that the nodal surface of the second $^2P^o$ state is not due to the symmetry of the state but the excitation of the angular mode [21]. The $^2P^o(T=0)$ component contains two nodal surfaces due to symmetry. Thus in comparison the $T=0$ component is less easily excited and it contributes only about 10% to the total density.

While the nondominant T components do not contribute significantly to the total shape densities, it is interesting to examine their shape densities nonetheless. For the four states in the first group, besides the dominant coplanar equilateral triangular geometry, there are basically three other types of density profiles among the T components. The first is for those which satisfy Eq. (13) but not Eq. (14). This is exemplified by the $^2D^e(T=1)$ and $^2D^o(T=2)$ components. Its density vanishes when the plane of the three electrons contains the nucleus, i.e., the density vanishes when $\theta=\pi/2$. In other words, coplanar structure is not allowed. The second type is for those which satisfy Eq. (14) but not Eq. (13). This type of density is exemplified by the $^2D^e(T=0)$ component. Here the three electrons are allowed to be coplanar with the nucleus. However, the three electrons are not allowed to form an equilateral triangle ($\eta=2\pi/3$, $\phi=0$). The third type is for the states which satisfy both Eq. (13) and Eq. (14). The examples are the $^4P^e(T=1)$, $^2P^o(T=0)$, and $^2D^o(T=0)$ components. The three-electron density is characterized by a nodal plane for $\theta=\pi/2$, as well as when the three electrons form an equilateral triangle. In other words, it is a combination of the two types above.

To provide a clearer view of the graphs which contain a node at $\theta=\pi/2$, we show two expanded views of the contour surfaces for the $^4S^o(T=0)$ and $^2P^o(T=0)$ components in Figs. 7(a) and 7(b), respectively. The plane of the triangles is for $\theta=\pi/2$, i.e., the coplanar geometry with the nucleus. In Fig. 7(a) the two contour surfaces of 60% of the maximum lie above and below the plane and the maximum density lies inside each surface. This figure clearly illustrates that the three electrons form an equilateral triangle but it cannot be coplanar with the nucleus. Figure 7(b) provides a detailed view which shows the three electrons can form neither coplanar geometry nor an equilateral triangle.

Comparing to the dominant T component, the density functions for the nondominant T components have additional nodal surfaces. When the three electrons form a coplanar equilateral triangle, it has the smallest electron repulsion energy. When the three electrons are not allowed to form a coplanar equilateral triangle the Coulomb repulsion energy will be greater. For each of the four states in the first group, it happens that it is always possible to find a T component where the coplanar equilateral triangle is allowed. For such states, that T component will be the dominant component. The other T components have nodal surfaces and thus have higher energies and they are not ''occupied'' by the low-lying states.

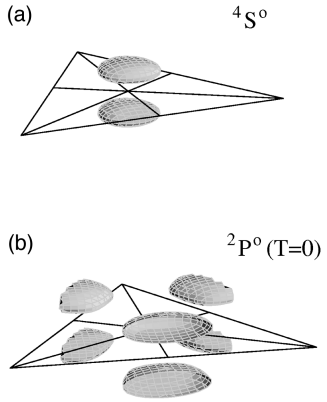

FIG. 7. Expanded views of the equidensity surface plots which show the existence of a nodal surface at $\theta=\pi/2$, i.e., when the nucleus and the three electrons are coplanar. This plane is represented by the plane of the paper in the figures. The equidensity surfaces exist in pairs, one above the plane and the other below the plane, but the density vanishes on the plane.

The above analysis indicates that each intrashell $2l2l'2l''$ triply excited state has one dominant T component when the three electrons are at the same distance from the nucleus. When the three electrons are at different distances from the nucleus, we can still define the plane formed by the three electrons and define the quantization axis to be perpendicular to this plane. [See Eq. (11).] However, the shapes of the system become more complicated. Two of the constraints from the quantum symmetry, Eqs. (14) and (15), are also lost. However, the discussion of the densities above for the limit of $r_1=r_2=r_3$ is still qualitatively valid even when the

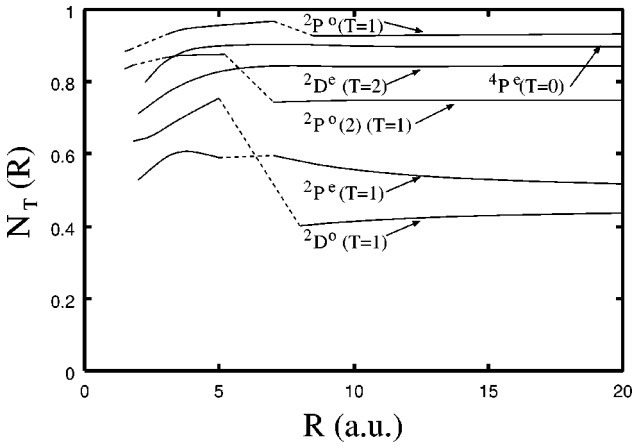

FIG. 8. Purities of the dominant T component as a function of R for the six $2l2l'2l''$ triply excited states of Li. The purity for the $^2P^e$ is not good as explained in the text. The dashed lines represent the region where diabatic crossing among the potentials for triply excited states has been applied.

radial distances of the three electrons are slightly different since we expect the density not to vary rapidly. A partial verification is to examine the partial normalization constant $N_T(R)$ for each state defined by Eq. (17). This has been calculated for the six $L \neq 0$ intrashell state (thus more than one T component) in the $N=2$ manifold. In Fig. 8 we show the calculated fraction of the dominant T component for each of these six states as a function of the hyperradius R. Clearly the purities for the $^2P^o$, $^4P^e$, $^2D^e$ states, as well as the second $^2P^o$ state, are all very good, just nearly identical to the purities obtained when the three electrons are at the same distance from the nucleus. The purity for the $^2P^e$ state is not very good, as explained above. The purity for the $^2D^o$ state undergoes a large change between $R=5$ and 8 a.u. because of an avoided crossing with another adiabatic potential which supports triply excited states in this R region. The result above illustrates that the partial normalization constant $N_T(R)$ does not change significantly even when the radial distances of the three electrons from the nucleus begin to deviate from each other. This purity is essential for the energies of the states within the same group to form a rotor structure similar to that of an oblate symmetric top [23].

VII. SUMMARY AND CONCLUSIONS

In this paper we have analyzed the correlation properties of the doubly excited states and the triply excited states of a three-electron atom such as Li. By examining the hyperspherical channel functions, we showed that manifolds of doubly excited states and those of triply excited states can be distinguished by the distribution of the radial distances of the three electrons, or in terms of the hyperspherical angles α_1 and α_2. Within the same manifold, the states are distinguished by the relative angles among the electrons. For doubly excited states we illustrated that if the motion of the innermost electron is averaged out, the correlations of the two outer electrons are essentially identical to those in the doubly excited states of the two-electron atom. Thus the same set of quantum numbers for describing doubly excited states of He can be used directly to describe the doubly excited states of Li. For triply excited states we analyze the shape of the three electrons when the three electrons are at the same distance from the nucleus. By examining the wave functions in the body frame, we were able to identify the various modes of internal vibrations of the three electrons. By sorting out states that have similar densities, these states are then shown to display rotor structure similar to that for a symmetric top.

ACKNOWLEDGMENTS

We thank Dr. Y. Li and Dr. E. Y. Sidky for useful discussions. This work was supported in part by the U.S. Department of Energy, Office of Basic Energy Research, Division of Chemical Sciences.

[1] D. R. Herrick, M. E. Kellman, and R. D. Poliak, Phys. Rev. A **22**, 1517 (1980).
[2] M. E. Kellman and D. R. Herrick, Phys. Rev. A **22**, 1536 (1980).
[3] G. S. Ezra and R. S. Berry, Phys. Rev. A **28**, 1974 (1983).
[4] C. D. Lin, Phys. Rev. A **29**, 1019 (1984).
[5] S. Watanabe and C. D. Lin, Phys. Rev. A **34**, 823 (1986).
[6] J. Z. Tang, S. Watanabe, and M. Matsuzawa, Phys. Rev. A **46**, 2437 (1992).
[7] J. Z. Tang, S. Watanabe, M. Matsuzawa, and C. D. Lin, Phys. Rev. Lett. **69**, 1633 (1992).
[8] B. Zhou, C. D. Lin, J. Z. Tang, S. Watanabe, and M. Matsuzawa, J. Phys. B **26**, 2555 (1993).
[9] B. Zhou and C. D. Lin, J. Phys. B **26**, 2575 (1993).
[10] O. I. Tolstikhin, S. Watanabe, and M. Matsuzawa, J. Phys. B **29**, L389 (1996).
[11] D. Kato and S. Watanabe, Phys. Rev. A **56**, 3687 (1997).
[12] T. Morishita and C. D. Lin, Phys. Rev. A **57**, 4268 (1998).
[13] J. Macek, J. Phys. B **1**, 831 (1968).
[14] D. O. Harris, G. G. Engerholm, and W. D. Gwinn, J. Chem. Phys. **43**, 1515 (1965); A. S. Dickinson and P. R. Certain, *ibid.* **49**, 4209 (1968); J. C. Light and R. B. Walker, *ibid.* **65**, 4272 (1976); J. C. Light, I. P. Hamilton, and J. V. Lill, *ibid.* **82**, 1400 (1985).
[15] M. Domke, C. Xue, A. Puschmann, T. Mandel, E. Hudson, D. A. Shirley, G. Kaindl, C. H. Greene, H. R. Sadeghpour, and H. Petersen, Phys. Rev. Lett. **66**, 1306 (1991).
[16] J. Z. Tang and I. Shimamura, Phys. Rev. A **50**, 1321 (1998).
[17] T. Morishita, O. I. Tolstikhin, S. Watanabe, and M. Matsuzawa, Phys. Rev. A **56**, 3559 (1997).
[18] M. Le Dourneuf and S. Watanabe, J. Phys. B **23**, 3205 (1990).
[19] R. G. Littlejohn and M. Reinsch, Phys. Rev. A **52**, 2035 (1995).
[20] S. Watanabe and C. D. Lin, Phys. Rev. A **36**, 511 (1987).
[21] C. G. Bao, X. Z. Yang, and C. D. Lin, Phys. Rev. A **55**, 4168 (1997).
[22] Z. Chen, C. G. Bao, and C. D. Lin, J. Phys. B **25**, 61 (1992).
[23] T. Morishita, Y. Li, and C. D. Lin, Phys. Rev. A **58**, 4214 (1998).